Condensation from Steam–Air Mixtures in a Horizontal Annular Flow Channel

G. Nolte and F. Mayinger
Technische Universität München
Lehrstuhl A für Thermodynamik,
Munich, West Germany

■Experiments were performed on the condensation of steam from steam–air mixtures in annular flow at a cooled inner tube. The range of investigation was varied for laminar and turbulent flow for $1.5 \times 10^3 \leq \mathrm{Re} \leq 1.3 \times 10^4$ and inlet concentrations $0.59 \leq p_{steam}/p_{total} \leq 0.95$. The measurements, performed at an open test loop at $p_{total} \approx 0.96$ bar, allowed local heat and mass transfer coefficents to be evaluated for various inlet lengths in the 2 m long annulus. The steam concentration was measured locally inside the annulus with a newly developed dew-point probe. The heat flux was measured locally using the temperature gradient in the cooled inner tube.

Near the inlet region the experiments showed a slightly higher heat flux at the bottom of the tube compared to the top, although it is expected to be smaller there owing to a thicker liquid film. Far downstream from the inlet region the heat transfer at the top was higher than at the bottom. The reasons for these effects are discussed, yielding a better understanding of the thermal and fluid processes involved in condensation from vapor–gas mixtures. The measured data allow the development of correlations for predicting the local Nusselt and Sherwood numbers in a horizontal annular-flow channel.

Keywords: *condensation, steam–air mixtures, annular flow*

INTRODUCTION

The process of condensation in the presence of noncondensables is encountered in a great number of technical apparatuses in the chemical and energy industries. For example, in heat exchangers even a small amount of noncondensable gas has a strong influence on the transferred energy flow.

Experimental investigations on partial condensation are not very numerous. Marschall [1] and Lehr [2] described the heat and mass transfer from binary mixtures at the inner side of a cooled vertical tube. Ackermann [3] investigated the condensation from steam–air mixtures inside a single vertical tube. The condensation of different vapors in the presence of air was researched by Gerhart [4] in a vertical mounted annulus, with the inner tube cooled. Dallmeyer [5] investigated partial condensation with special emphasis on the laminar and turbulent boundary layers at a vertical flat plate with longitudinal flow.

The above-mentioned experimental studies were carried out with different test sections, but all were vertically mounted with a vertical flow direction. The work reported here investigated the mechanism of heat and mass transfer along a cooled horizontal tube with the condensation of steam from a steam–air mixture in an annular-flow channel. The heat and mass transfer are mainly influenced by the condensing film flowing around the inner cooled tube and an increasing air fraction from the bulk of the annulus (partial pressure p_a) to the film surface (p_{af}). In contrast to pure steam condensation, the steam is transferred by convection and diffusion, and also a temperature profile (t_g–t_f) in the gas phase can be observed (see Fig. 1). Results on the condensation of steam out of steam–air mixtures at laminar and turbulent annular flow with varying inlet concentrations will be presented.

EXPERIMENTAL SETUP

The measurements of condensation in the presence of an inert gas were performed at an open test loop consisting mainly of the following equipment (Fig. 2): an electrically heated boiler producing the steam, a pressurized air tank, an air heater, a heat exchanger including the measuring section, and a cooling water supply.

The steam and air flow rates were measured separately in calibrated orifice flowmeters. The air passes an electric heater before being mixed with the steam and then enters the heat exchanger. To avoid condensation on the way to the test section, the steam is superheated to a higher pressure in the boiler.

The heat exchanger consists of two concentric tubes. The inner tube is cooled with water, and the outer tube is insulated. The condensing gas mixture flows through the annulus between the outer and inner tubes (hydraulic diameter $d_h = 2s = 15.5 \times 10^{-3}$ m).

To enable local measurements of heat and mass transfer along the heat exchanger tube with a condensing length of 2 m, an instrumented section 0.25 m long was installed, and the gas inlet was constructed to be movable in the axial direction. This was achieved by placing a pipe consisting of two concentric tubes in the gas annulus.

As shown in Fig. 2, the steam–air mixture passes through

Address correspondence to Prof.-Dr.-Ing. F. Mayinger, Technische Universität München, Lehrstuhl a für Thermodynamik, Arcistrasse 21, 8000 München 2, West Germany.

Experimental Thermal and Fluid Science 1988; 1:373-384

0894-1777/88/$3.50

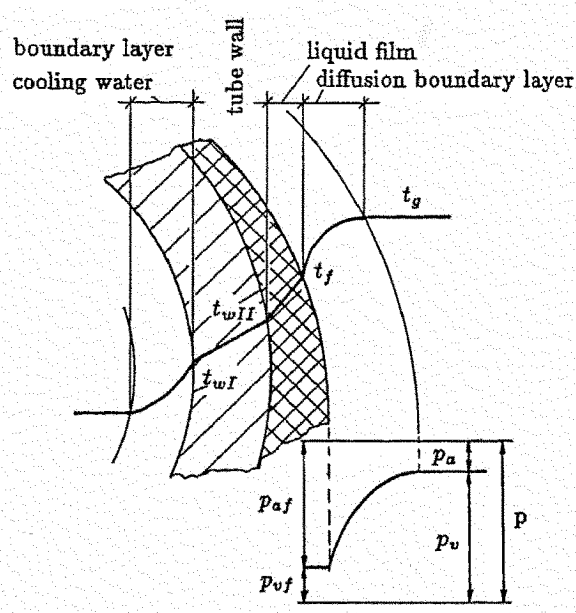

Figure 1. Temperature and partial pressure curve at partial condensation.

the pipe that is insulated by an air space from the water-cooled tube to avoid condensation on its way through before it enters the condensing flow path. The distance between the onset of condensation and the inlet of the measuring section could be varied by this device from 0 m up to 1.75 m in 0.25 m steps in order to get eight measuring intervals within a total length of 2 m.

The Test Section

The test section, illustrated in Fig. 3, has a condensing length of 0.25 m and is part of the heat exchanger described above. The temperatures of the gas mixture at the inlet and the outlet are measured with two thermocouples as t_{g1} and t_{g2}, respectively, to give a temperature difference expressed as $t_{g1} - t_{g2}$.

The wall heat flux through the water-cooled stainless steel tube (0.025 m × 0.015 m I.D.) can be calculated from the wall temperatures of the tube. Four thermocouples (0.5×10^{-3} m in diameter) are soldered in the wall—two at the outer surface (tw_{II}) and two at the inner surface (tw_I) of the tube. In order to get the circumferential temperature distribution, the tube can be turned. Figure 4 shows a cross section through the middle of the measuring section, where the cooled inner tube surrounded by a turnable ring can be seen. Two measuring divices are installed in this ring: a pressure tap, measuring the total pressure p and a dew-point probe for the determination of the steam–air fraction in the radial and circumferential directions.

MEASURING TECHNIQUE

Dew-Point Probe

The aim of the newly developed dew-point probe is to obtain the local concentration of noncondensables in a condensing atmosphere. The measurement is based on the determination of

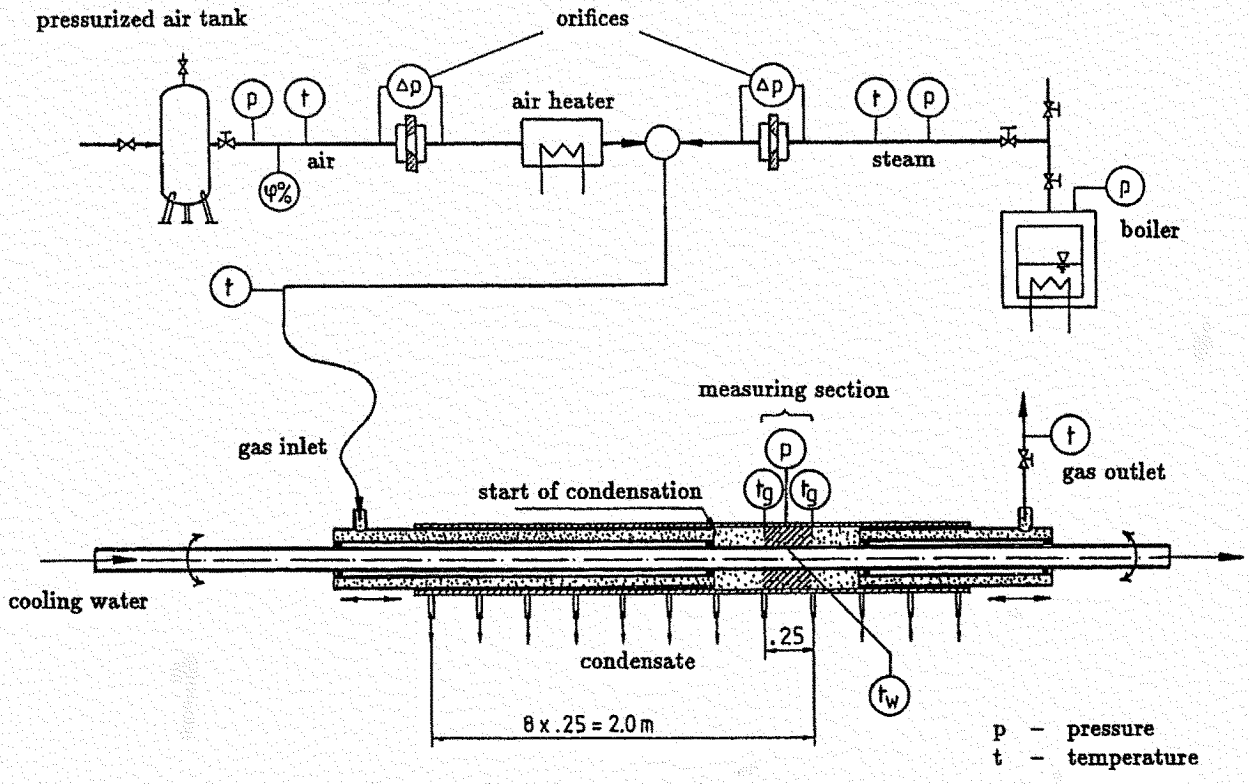

Figure 2. Experimental setup.

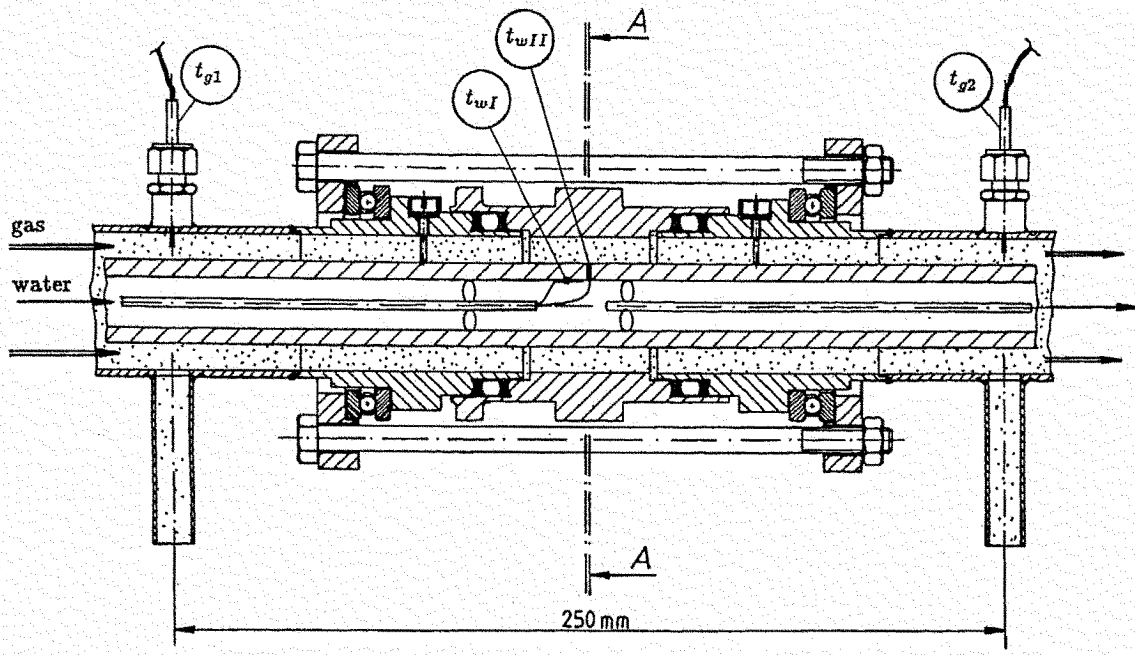

Figure 3. Test section.

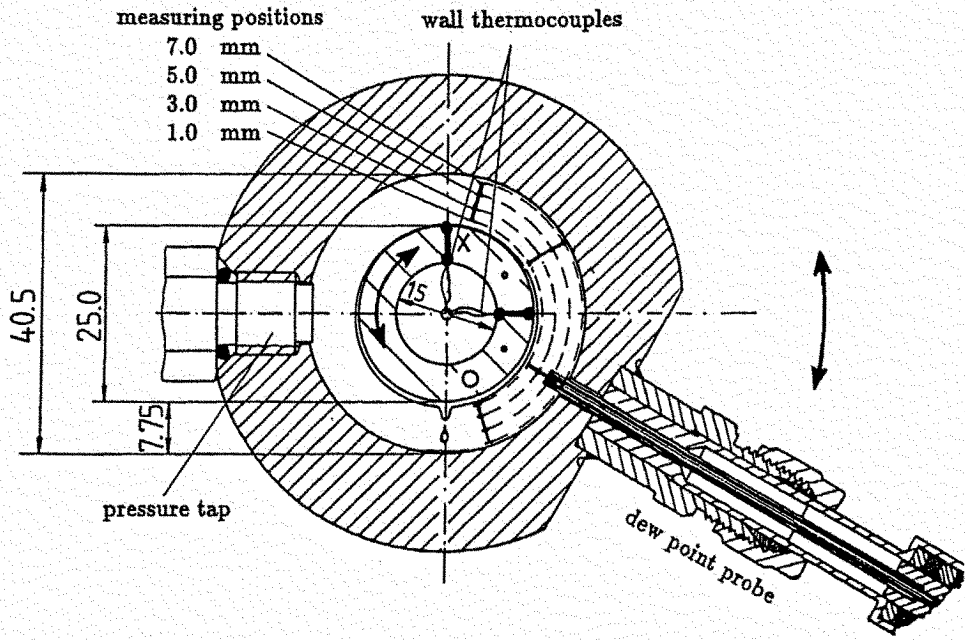

Figure 4. Cross section *A–A* through the middle of the measuring section.

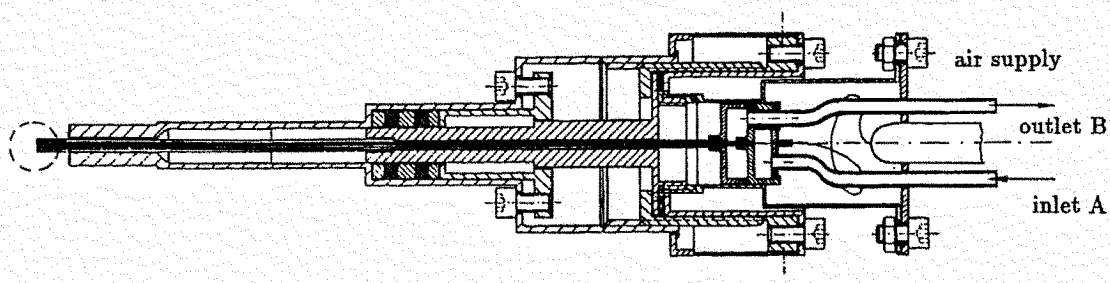

Figure 5. Dew-point probe.

the dew-point temperature t' and the total pressure p of the gas mixture.

Assuming the validity of the ideal gas law, we can calculate the mass ratio m_{nc}/m_c of the noncondensing gas (here, air) and the condensing gas (here, steam):

$$\frac{m_{nc}}{m_c}=\frac{p-p_c}{p_c}\left(\frac{R_c}{R_{nc}}\right)=\frac{1-\psi_c}{\psi_c}\left(\frac{R_c}{R_{nc}}\right) \tag{1}$$

with R_c and R_{nc} the specific gas constants and ψ_c the pressure ratio of the partial pressure p_c of the condensing gas to the total pressure p:

$$\psi_c=p_c/p \tag{2}$$

Since the total pressure p does not exceed about 10 bar and the presence of the noncondensing gas has negligible influence on the saturation partial pressure p_c', the unknown partial pressure p_c can be assumed to be equal to the saturation pressure p_c' at the dew-point temperature t' of the gas mixture. That is to say,

$$p_c=f(t') \tag{3}$$

The dew-point temperature t' can be measured with the probe shown in Fig. 5. The measuring sensor is a device consisting of a miniature thermocouple soldered to a copper foil about 0.1×10^{-3} m thick that separates the steam atmosphere from an inner channel system (see Fig. 6) through which the copper foil can be cooled with air from the rear. The inner capillary tubes of the channel system are connected to an air supply with an inlet A and an outlet B (Fig. 5). The two outer capillary tubes form an insulating space to avoid condensation at the outer tube wall of the probe.

As soon as the air cooling is begun, the temperature at the copper foil falls. Figure 7 shows three typical temperature curves recorded with a continuous line recorder. Curve 1 was detected in a pure steam flow, curve 3 in a pure air flow, and curve 2 in a mixture of steam and air. Curve 2 shows, after the start of cooling, a smooth decrease in the temperature until condensation begins on the outside of the copper foil, when a sudden strong change in the gradient can be observed. This marks the dew-point temperature from which the steam concentration of the investigated gas mixture can be calculated.

The scattering of the temperatures read out from the strip charts at the points of strong gradient change lies within ± 0.25 K; resulting in uncertainties for ψ ranging from $\Delta\psi \approx \pm 0.01$ (for $\psi = 0.95$) to $\Delta\psi \approx \pm 0.002$ (for $\psi = 0.1$).

EVALUATION

The varying heat and mass transfer in the axial direction is influenced mainly by a decreasing steam flow rate,

$$\dot{M}_{v2}=\dot{M}_{v1}-|\dot{M}_{\text{cond}}| \tag{4}$$

and a constant airflow rate,

$$\dot{M}_{a2}=\dot{M}_{a1}=\text{constant} \tag{5}$$

further a temperature and air fraction profile in the radial direction in the gas phase.

The total heat transfer from the gas to the cooled wall is controlled by three heat transport phenomena:

1. $\dot{Q}_m$ due to the phase change of the condensing steam at the film surface
2. $\dot{Q}_a$ due to the convection in the gas annulus
3. $\dot{Q}_c$ due to the convective transport in the liquid film

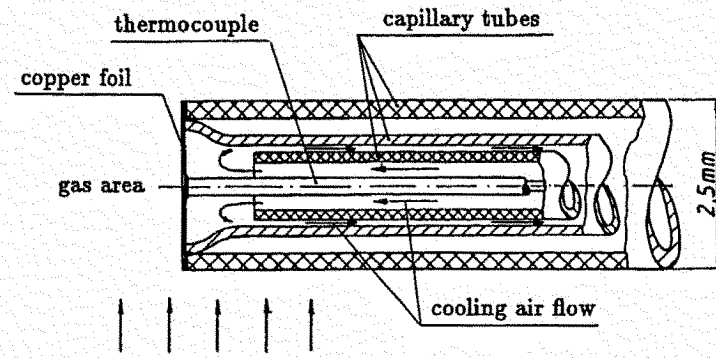

Figure 6. Top of the dew-point probe.

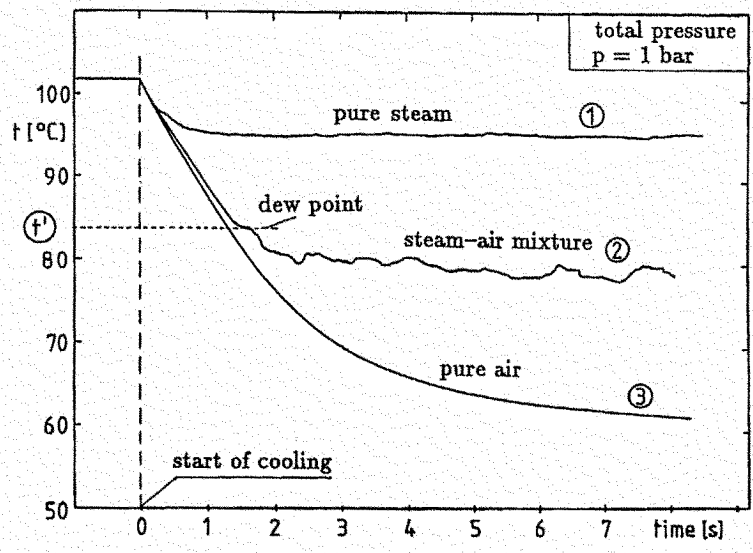

Figure 7. Temperature curve at the top of the dew-point probe in (1) pure steam, (2) a steam–air mixture, and (3) pure air.

Neglecting axial heat transfer in the cooled tube, the total heat flux $\dot{Q}_w$ can be expressed by

$$\dot{Q}_w = \dot{Q}_m + \dot{Q}_d + \dot{Q}_c \tag{6}$$

Combining the energy balance at the liquid film (see Fig. 8),

$$\Delta\dot{Q}_w = \dot{M}_c h_c - \left(\dot{M}_c + \frac{d\dot{M}_c}{d\varphi}\Delta\varphi\right) h_{c|\varphi+\Delta\varphi} + \Delta\dot{Q}_f \tag{7}$$

with the energy balance in the gas annulus (see Fig. 9),

$$\Delta\dot{Q}_f = \Delta\dot{M}_a\, h_{a1} - \Delta\dot{M}_a\, h_{a2} + \Delta\dot{M}_{v1}\, h_{v1} - \Delta\dot{M}_{v2}\, h_{v2} - \Delta\dot{M}_c\, \Delta h_v[t_f] \tag{8}$$

the total heat flux $\tilde{\dot{Q}}_w$ averaged over the length of the measuring section becomes

$$\left.\begin{aligned}\tilde{\dot{Q}}_w = {} & \tilde{\dot{M}}_{\text{cond}}\,\Delta h_v[t_f] && \Big\}\ \tilde{\dot{Q}}_m\\ & + (\dot{M}_a c_{pa} + \tilde{\dot{M}}_v c_{pv})(t_{g1} - t_{g2}) && \Big\}\\ & + \tilde{\dot{M}}_{\text{cond}} c_{pv}(\tilde{t}_g - \tilde{t}_f) && \Big\}\ \tilde{\dot{Q}}_d\\ & + \tilde{\dot{M}}_{\text{cond}} c_c(\tilde{t}_f - \tilde{t}_{\text{cond}}) && \Big\}\ \tilde{\dot{Q}}_c\end{aligned}\right. \tag{9}$$

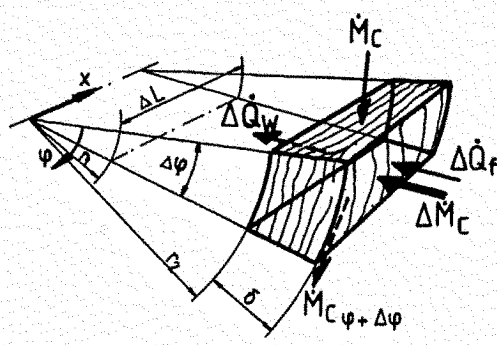

Figure 8. Reference volume at the liquid film.

where a tilde (˜) indicates a mean value. In Eq. (9) the wall heat flux $\dot{Q}_w$, the condensate flux $\dot{M}_{\text{cond}}$, the temperature $\tilde{t}_f$ at the film surface and the temperature $\tilde{t}_{\text{cond}}$ of the dropping film at the bottom of the tube are unknown.

The wall heat flux $\dot{Q}_w$ can be calculated from the measured wall temperatures t_{w_I} and $t_{w_{II}}$:

$$\dot{Q}_w = \frac{\lambda_w}{r_2 \ln(r_2/r_1)}\, 2\pi r_2\, \Delta L\, (\tilde{t}_{w_{II}} - \tilde{t}_{w_I}) \tag{10}$$

In contrast to the Nusselt Wasserhauttheorie, the film surface temperature t_f cannot be assumed to be constant, and also the influence of the condensate subcooling ($t_f - t_{\text{cond}}$) cannot be neglected. It can be calculated from the energy balance at the laminar film (see Fig. 10),

$$\frac{\partial\dot{H}}{\partial\varphi}\Delta\varphi + \frac{\partial\dot{Q}}{\partial r}\Delta r = 0 \tag{11}$$

combined with the momentum balance, yielding the differen-

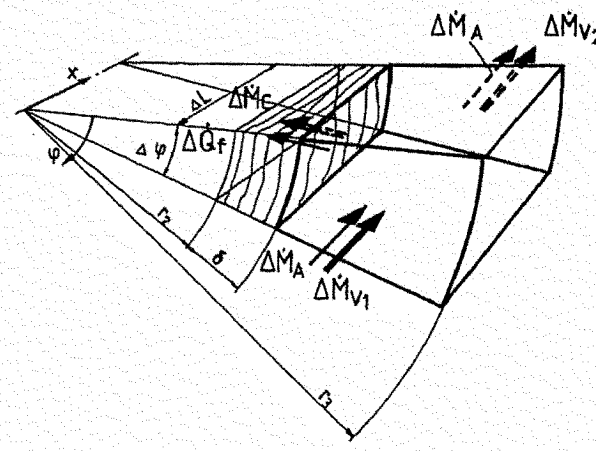

Figure 9. Reference volume at the gas annulus.

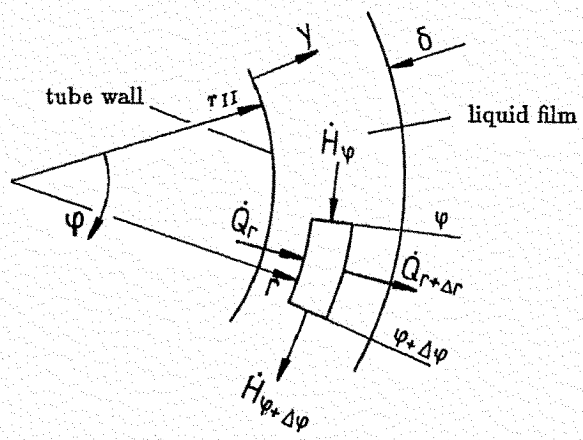

Figure 10. Energy balance in the liquid film.

tial equation

$$\frac{\partial}{\partial\varphi}\left[\frac{\rho_c^2 g\sin\varphi}{\eta_c}\left(\delta_\varphi y-\frac{y^2}{2}\right)c_c t\right]+\frac{\partial}{\partial r}\left(\lambda_c r\frac{\partial t}{\partial r}\right)=0 \quad (12)$$

which can be solved numerically. The film thickness δ_φ can be calculated from

$$\delta_\varphi=\left(\frac{\dot{M}_c(\varphi)(3\eta_c)}{\rho_c^2 g\,(\sin\varphi)\,\Delta L}\right)^{1/3} \quad (13)$$

Definition of the Nusselt and Sherwood Numbers

The resistance for the transport of the "dry" heat flux $\dot{Q}_d$ from the bulk of the gas flow to the film surface can be described by the so-called dry heat transfer coefficient α_d according to

$$\tilde{\dot{Q}}_d=\alpha_d(2\pi r_2\,\Delta L)\,(\tilde{t}_g-\tilde{t}_f) \quad (14)$$

The resistance to the heat flux $\dot{Q}_m$ is described by the mass transfer coefficient β according to

$$\dot{Q}_m=\beta\frac{p}{R_v}\left[\left(\frac{\bar{\psi}_v}{T_v}\right)_g-\left(\frac{\bar{\psi}_v}{T_v}\right)_f\right](2\pi r_2\Delta L) \quad (15)$$

The heat transfer is characterized by the Nusselt number (Nu), defined by

$$\mathrm{Nu}=\frac{\alpha_d(2s)}{\lambda_g} \quad (16)$$

and the mass transfer by the Sherwood number (Sh)

$$\mathrm{Sh}=\frac{\beta(2s)}{D} \quad (17)$$

Table 1. Inlet Conditions of the Steam–Air Mixtures

Run	ψ_{in}	Re_{in}	$t_{g,in}$ (°C)	p (bar)
1	0.95	7.9×10^3	104	0.96
2	0.78	7.9×10^3	104	0.96
3	0.59	7.9×10^3	104	0.96

EXPERIMENTAL RESULTS

The results of three arbitrary selected experimental runs are presented. The inlet conditions can be characterized by the Reynolds number

$$\mathrm{Re}=\frac{w_g(2s)}{\nu_g} \quad (18)$$

the steam–air fraction $\psi_{in}=p_{steam}/p_{total}$, the temperature t_g of the gas mixture, and the total pressure p. The varying parameter in these runs was the pressure ratio ψ_{in} at the inlet as a measure for the steam fraction ranging from 0.59 to 0.95 as can be seen in Table 1.

In Fig. 11, Re is plotted versus the condensing length l. Due to the condensation of the steam, all three runs show a decrease in Re. The higher decrease of the Reynolds number in run 1 compared to runs 2 and 3 can be explained by a lower air mass

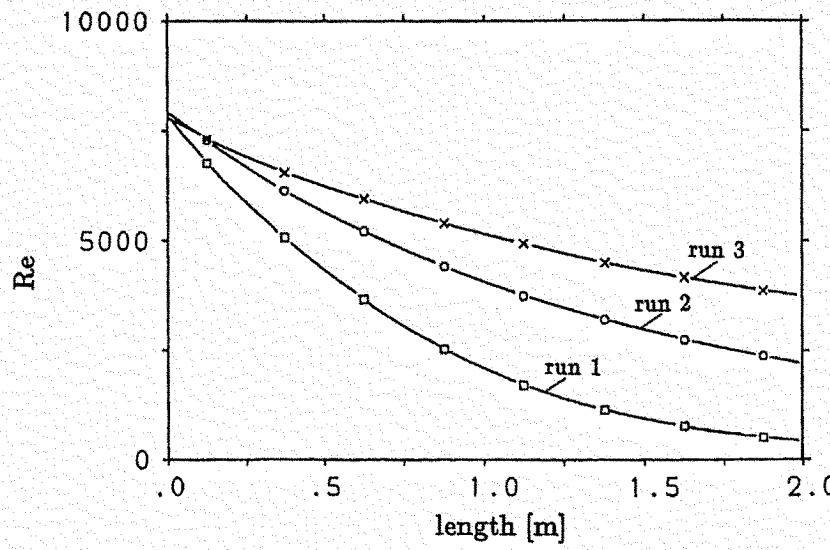

Figure 11. Reynolds number ($d_h = 2s$) versus the tube length.

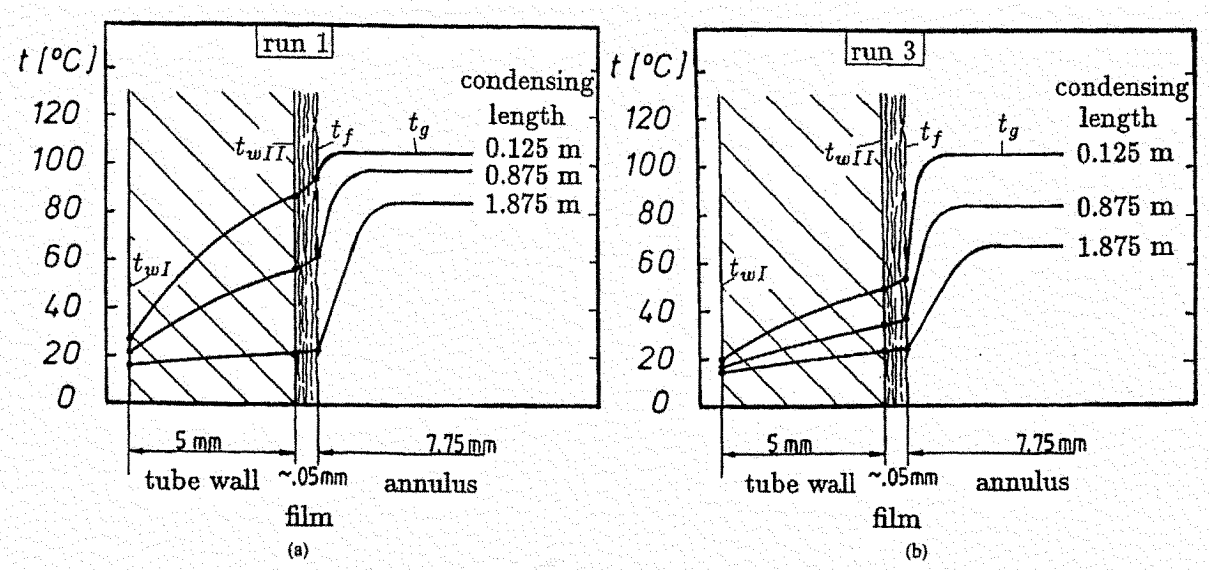

Figure 12. Temperature curve from the inner water-cooled tube to the gas annulus for run 1 (a) and run 3 (b).

flow rate due to the different concentrations ψ_{in} at the inlet. The corresponding gas velocities for run 1 range from 11.0 m/s at the inlet to 0.65 m/s at the outlet.

Figures 12*a* and *b* show the temperature curve from the inner water-cooled tube wall through the water film to the bulk of the gas mixture. The radial data were taken at three different axial positions—0.125, 0.875, and 1.875 m from the inlet of the annulus. The temperature t_g of the gas mixture and the wall temperatures tw_I, tw_{II} were measured. The temperature t_f at the film surface was calculated from the energy and momentum balance in the film, Eqs. (11) and (12).

The temperature difference $(t_g - t_f)$ between the gas mixture and the film surface is used when defining the convective dry heat transfer coefficient. The total heat flux can be calculated from the temperature gradient in the material of the tube wall.

In Fig. 13 the heat flux density averaged over the circumference of the tube is plotted versus tube length. After a flow path of approximately 1.5 m, most of the steam in the gas mixture has been condensed, and the curves of the three different inlet steam concentrations tend to fall together.

An impression of the mean steam concentration in the annulus and at the surface of the liquid film can be derived from Fig. 14. It shows the pressure ratio ψ_m averaged over the circumference of the annulus versus the condensing length. The pressure ratio at the film surface (dotted lines) was evaluated from the calculated temperature at the film surface derived from Eqs. (11) and (12) assuming saturated vapor $\psi_f = p'_{steam}[t_f]/p$. The mean pressure ratio in the gas annulus was calculated from the energy and mass balance and also measured with the dew-point probe. The measured and calculated curves show very good agreement. The deviation

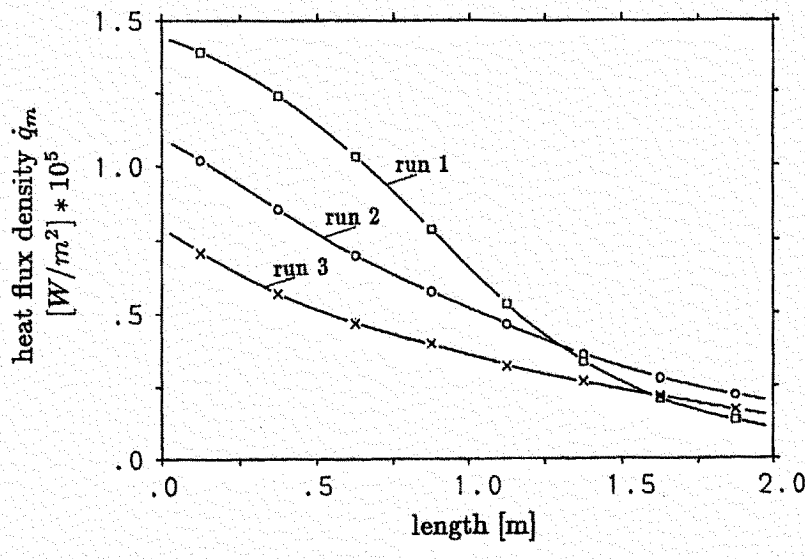

Figure 13. Mean total heat flux density $\dot{q}_m$.

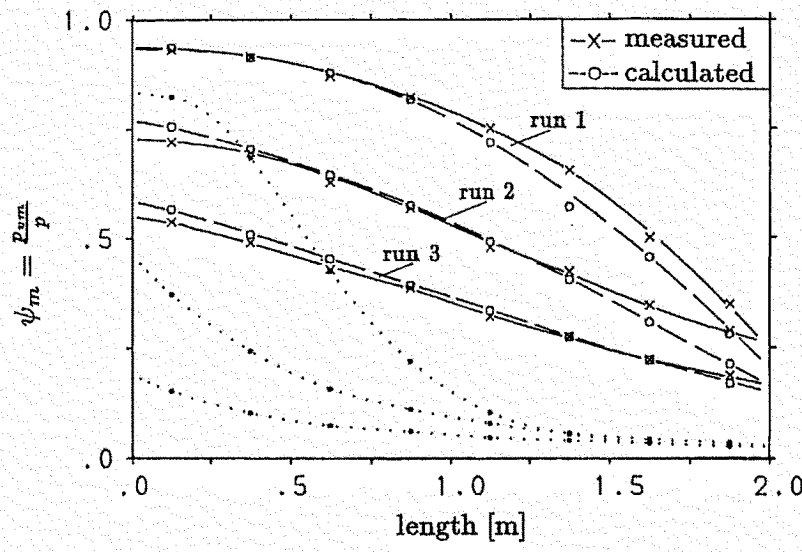

Figure 14. Pressure ratio $\psi_m = p_{v,\text{mean}}/p_{\text{total}}$ in the gas annulus (——) and at the film surface (···).

can be explained by an error of less than 2% in the measurement of the steam or air flow, respectively.

In order to describe the mass transfer to the cooled tube, the concentration profile had been determined with the dew-point probe in the radial, circumferential, and longitudinal directions inside the annular flow channel. The measured data selected at three axial positions (0.125, 0.875, and 1.875 m from the inlet of the annulus) are demonstrated in Fig. 15, where $y = 0$ mm locates the film surface. As expected, the condensation at the cooled tube yields an increase in the concentration profile in the radial direction and a decrease in the axial direction.

An interesting effect can be observed in the profiles in the circumferential direction. An idea of what this profile looks like can be derived by comparing the concentrations at the top (15°) and bottom (165°) of the annulus at the same axial and radial position. At the inlet of the annulus the concentration profile is balanced over the circumference. With increasing condensing length, a higher concentration at the top compared to the bottom can be observed. Far downstream, when the steam–air flow is developing into a pure air flow with only a little saturated steam, the radial profile at the top and at the bottom tend to fall together, as can be seen in Fig. 15*c*, comparing the radial profiles at the end (1.875 m) and in the middle (0.875 m) of the annulus.

The local heat flux has been evaluated from the temperature gradient in the material of the cooled tube, which was determined with two thermocouples positioned near the inner and outer surfaces of the tube. In order to measure the heat flux profile over the circumference the tube was installed to be turnable. As expected, the heat flux profile depends on the thickness of the liquid film flowing around the cooled tube and on the turbulence of this film.

The thickness of the liquid film was calculated from Eq. (13) over the circumference of the tube and varied from 0.03–0.05 $\times 10^{-3}$ m at the top up to 0.1 $\times 10^{-3}$ m at the bottom as shown for runs 1–3 in Fig. 16 for two axial positions at the inlet and outlet of the tube. It should be noted that in this calculation the influence of the axial shear stress at the gas–liquid is not yet included.

Figure 17 shows the variation of the heat flux in the circumferential direction compared to the mean heat flux averaged locally over the surface of the tube. Due to the greater thickness of the liquid film at the bottom of the tube, the heat flux should be smaller there. Near the inlet region, however, the experiments showed a slightly higher heat flux at the bottom compared to the top. This tendency was observed for all three runs and is demonstrated for run 1 in Fig. 17. Due to the liquid separation at the bottom of the tube wall a higher turbulence can be observed, especially at the inlet region, where the flow turbulence and in particular the condensing mass flow rate are higher.

Far downstream from the inlet region the heat transfer at the top was higher than at the bottom. Along the flow path the gas velocity and also the condensing mass flow are decreasing, which reduces the momentum and shear transfer between the gas and the liquid film, yielding a lower turbulence in the film and also in the gas flow. In addition, the dew-point measurements showed in the axial direction a balanced profile over the circumference at the inlet of the annulus. Downstream the concentration of air at the bottom was increasing more than at the top, which yielded an additional resistance for the heat and mass transfer at the bottom of the tube.

Finally, the local Nusselt and Sherwood numbers describing the heat and mass transfer from the gas to the liquid film were calculated from the measured temperature and steam–air fraction according to Eqs. (14)–(17). The local mean values averaged over the circumference of the tube are plotted in Fig. 18 versus the tube length and in Fig. 19 versus the local Reynolds number.

Due to the higher turbulence and a higher condensing rate at the inlet, the curves show the typical developing flow from the inlet downstream throughout the condensing length. At the inlet the Nusselt and Sherwood numbers are rising from run 3 to run 1 with increasing steam fraction. Far downstream, most of the steam has been condensed and the heat and mass transfer is influenced mainly by the air mass flow so that the curves in Fig. 18 tend to fall together. The air mass flow, which is assumed to be constant over the tube length, is decreasing with increasing pressure ratio ψ_{in} from run 1 over run 2 to run 3. Due to a lower air mass flow, run 1 shows slightly lower

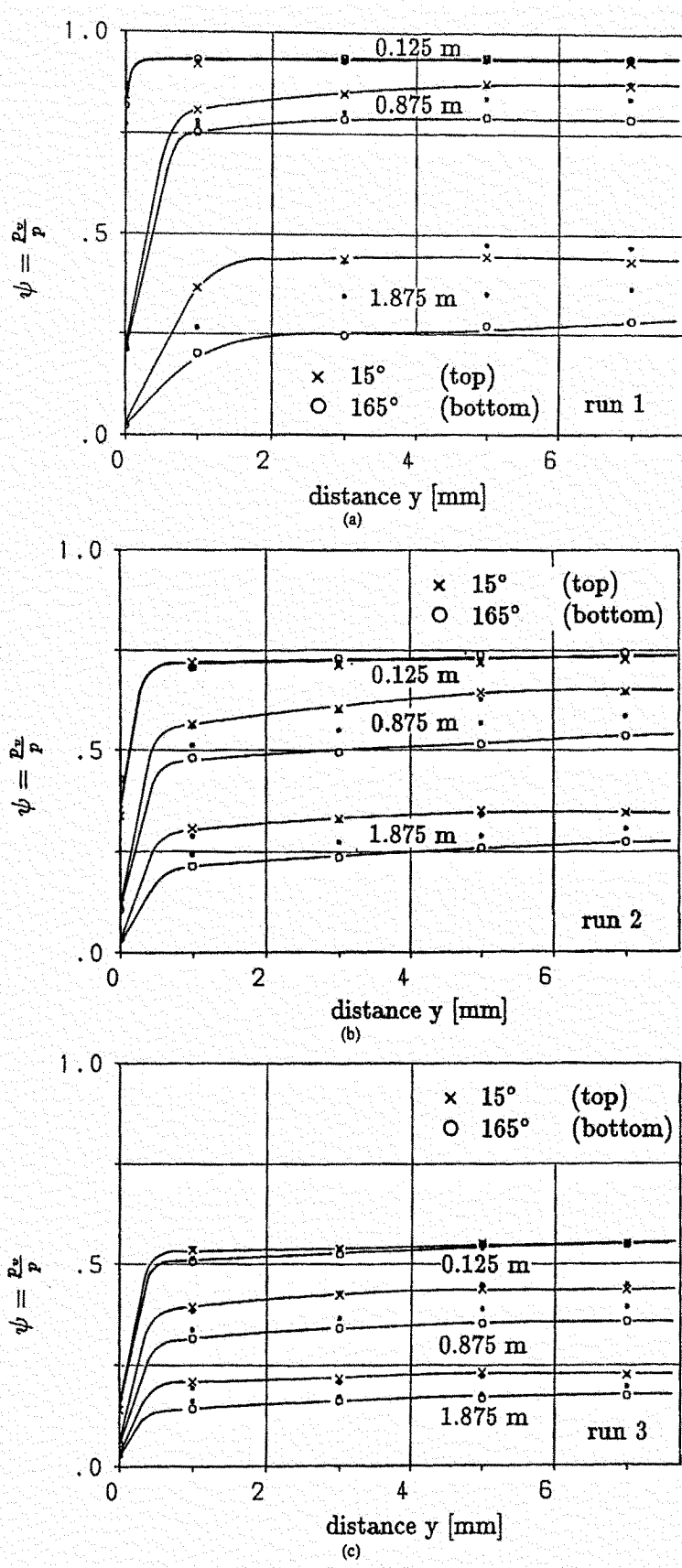

Figure 15. Pressure ratio $\psi = p_{steam}/p_{total}$ versus the distance of the film at three axial positions of the condensing length for run 1 (a), run 2 (b), and run 3 (c).

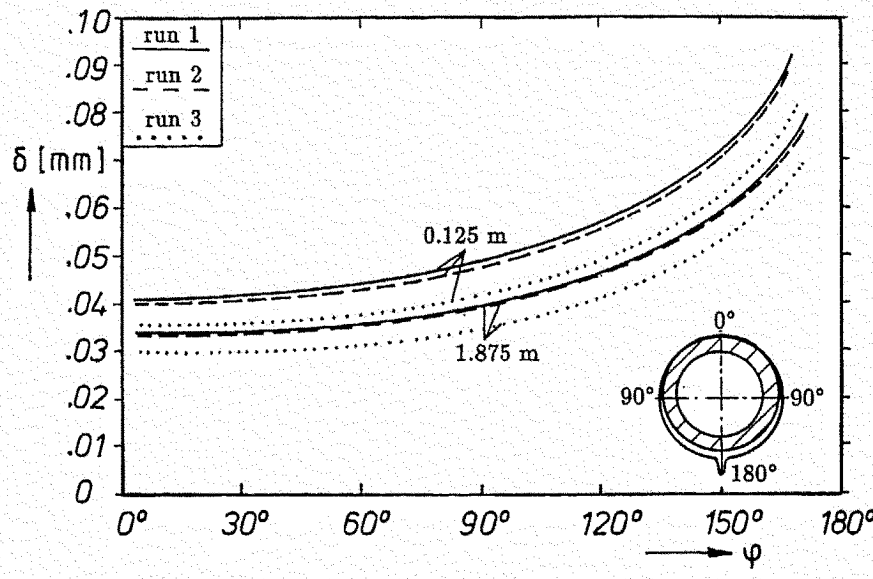

Figure 16. Calculated film thickness in circumferential direction at the inlet (0.125 m) and the outlet (1.875 m) of the annulus.

Nusselt and Sherwood numbers at the end of the tube compared to run 2 and run 3.

Analyzing the curves of the local Nu and Sh numbers versus the Re number in Fig. 19, we find a strong decrease in the Re number and in the heat and mass transfer due to the decreasing steam flow and decreasing gas velocity along the flow path.

CONCLUSIONS

Experiments on the condensation of steam out of steam–air mixtures in turbulent and laminar flow have been carried out in a horizontal annular flow channel. Temperature and concentration measurements were performed in radial, circumferential, and longitudinal direction at a 2 m long test section with varying inlet concentrations. The heat and mass transfer were described by the local Nusselt and Sherwood numbers versus the Reynolds number or versus the condensing length of the tube, respectively. The work for the future will be to develop correlations for predicting the Nusselt and Sherwood numbers for different steam–air fractions and varying Reynolds numbers.

NOMENCLATURE

c	specific heat capacity, J/(kg K)
d_h	hydraulic diameter, m
D	binary diffusion coefficient, m^2/s
$\dot{H}$	enthalpy flow, J/s
h	specific enthalpy, J/(kg K)
Δh_v	latent heat of condensation, J/(kg K)
Δl	length of the measuring section, m

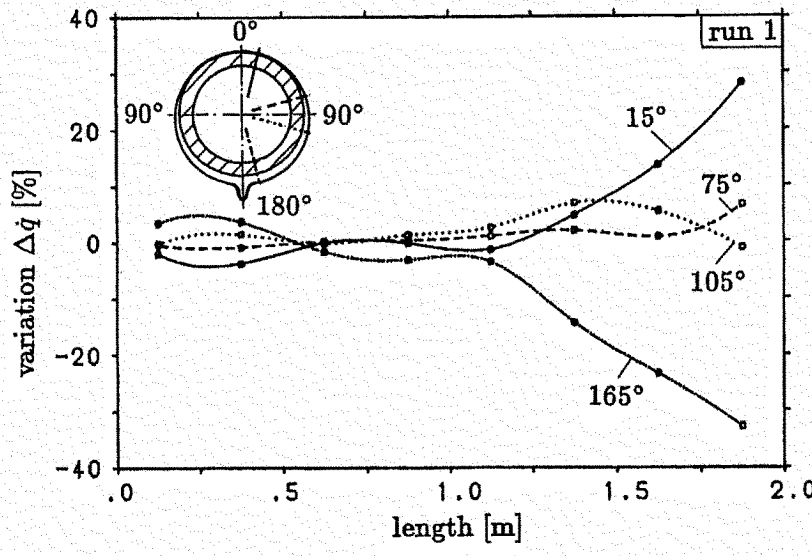

Figure 17. Variation $\Delta\dot{q}$ in the circumferential direction from the mean heat flux.

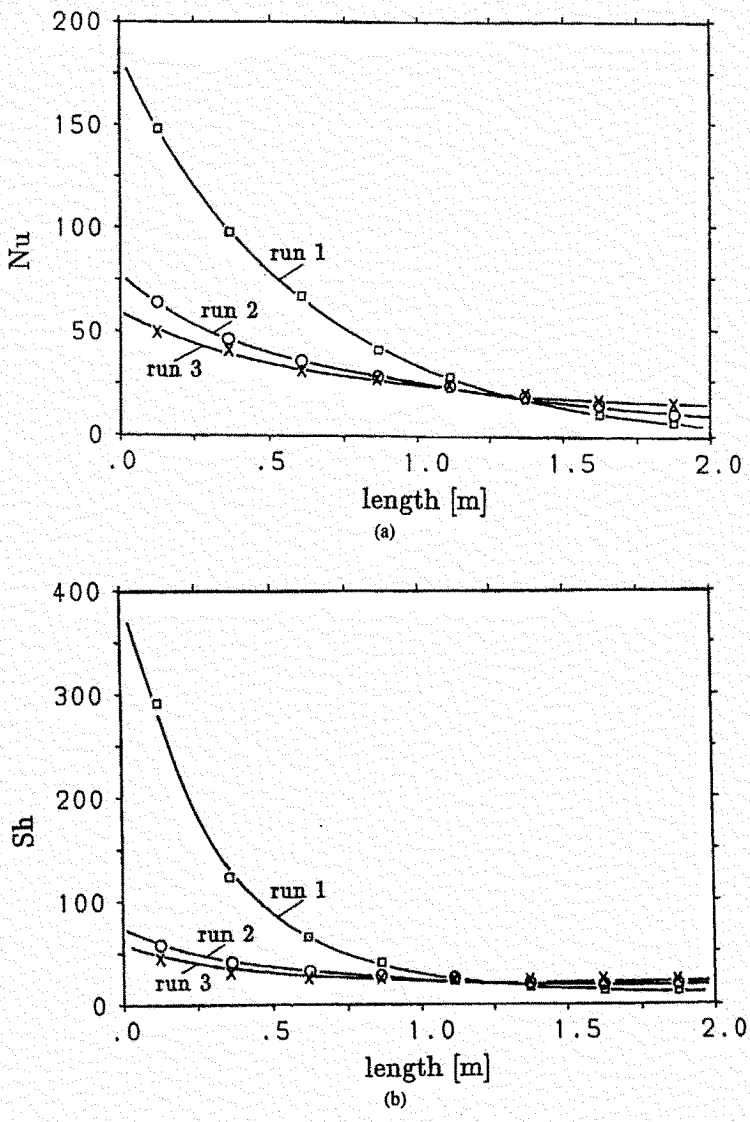

Figure 18. Nusselt (a) and Sherwood (b) numbers (mean values over the circumference) versus tube length.

m	mass, kg
$\dot{M}$	mass flow, kg/s
Nu	Nusselt number, Eq. (16), dimensionless
p, p_{total}	total pressure, N/m²
p_a	air pressure, N/m²
p_v	vapor pressure, N/m²
$\dot{Q}$	heat flux, W
$\dot{q}$	heat flux density, W/m²
w	velocity, m/s
R	ideal gas constant, J/(kgK)
r	radius, m
Re	Reynolds number, dimensionless
s	width of the annulus, m
Sh	Sherwood number, Eq. (17), dimensionless
t_{cond}	condensate temperature, °C
t_f	film surface temperature, °C
t_g	bulk temperature in the gas annulus, °C
t_w	wall temperature, °C
y	wall distance, m

Greek Symbols

δ_φ	condensate film thickness, m
λ	thermal conductivity, W/(mK)
φ	angle in circumferential direction, degrees
η	dynamic viscosity, kg/(ms)
ν	kinematic viscosity, m²/s
ρ	density, kg/m³
ψ	pressure ratio ($=p_{steam}/p_{total}$), dimensionless

Subscripts

1, 2	inlet, outlet of the measuring section
I, II	innersurface, outersurface of the cooled tube
a	air

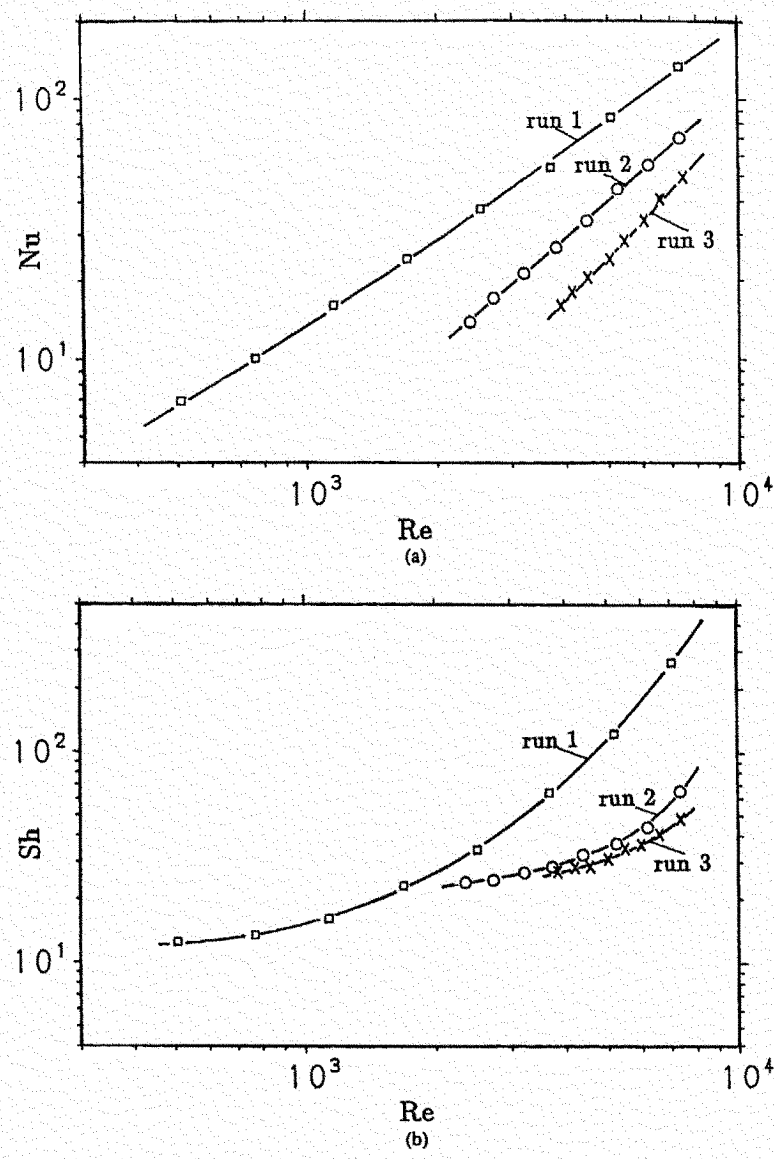

Figure 19. Nusselt (a) and Sherwood (b) numbers (mean values over the circumference) versus Reynolds number.

c	condensable
f	at the film surface
g	in the gas annulus
in	at the inlet
nc	noncondensable
v	vapor
w	at the tube wall

REFERENCES

1. Marschall, E., Wärmeübertragung bei der Kondensation von Dämpfen aus Gemischen mit Gasen. Abh. Dtsch. Kältetechnischer Verein Nr. 19 C. F. Müller, Karlsruhe, 1967.
2. Lehr, G., Wärme- und Stoffübertragung bei der Kondensation von zwei Dämpfen aus einem Gemisch mit einem Inertgas, Dissertation, Technical University, Hanover, 1972.
3. Ackermann, D., Wärme- und Stoffübertragung bei der Kondensation eines Dampfes aus einem Gemisch mit einem nicht kondensierbaren Gas in laminarer und turbulenter Strömungsgrenzschicht, Dissertation, Universität Stuttgart, 1972.
4. Gerhart, K., Stoff- und Wärmeübertragung bei der Kondensation von Dämpfen aus im Ringspalt strömenden Gemischen mit Luft, Dissertation, Technische Hochschule, Aachen, 1969; *VDI Forsch.* **539**, 25–48, 1969.
5. Dallmeyer, J., Stoff- und Wärmeübertragung bei der Kondensation eines Dampfes aus einem Gemisch mit einem nicht kondensierbaren Gas in laminarer und turbulenter Strömungsgrenzschicht, Dissertation, Technische Hochschule, Aachen, 1968; *VDI Forsch.* **539**, 4–24, 1968.

Received January 25, 1988; revised May 26, 1988